

# Single nozzle electrospinning of encapsulated epoxy and mercaptan in PAN for self-healing application

Sayed Ali Mirmohammad Sadeghi <sup>a</sup>, Sedigheh Borhani <sup>a,\*</sup>, Ali Zadhoush <sup>a</sup>, Mohammad Dinari <sup>b</sup>

<sup>a</sup> Department of Textile Engineering, Isfahan University of Technology, Isfahan 84156-83111, Iran

<sup>b</sup> Department of Chemistry, Isfahan University of Technology, Isfahan 84156-83111, Iran



## ARTICLE INFO

### Keywords:

Single nozzle electrospinning  
Phase separation  
Solubility parameter

## ABSTRACT

In this research, two types of core-shell nanofibers, epoxy-polyacrylonitrile (PAN) and mercaptan-PAN were successfully fabricated using single nozzle electrospinning. Fourier transform infrared spectroscopy (FTIR) analysis showed absence of chemical reaction between the encapsulated epoxy or mercaptan and PAN. Moreover, transmittance electron microscopy (TEM) images proved that the encapsulated epoxy and mercaptan were uniformly distributed within core of the nanofibers. Hybrid core-shell nanofibers mat was produced through twin electrospinning of epoxy-PAN and mercaptan-PAN on the same collector. Solidification of released core materials leads to repair a damaged area which could be used in epoxy composites for self-healing application. Degree of curing of epoxy resin was obtained to be 0.7 at 10 °C, proving that the dual component healing agent, epoxy and mercaptan is a suitable self-healing system in sub-room temperature. This research shows that solubility parameter of the materials plays a major role in the formation mechanism of core-shell nanofibers.

## 1. Introduction

Composite materials are used in many industrial applications due to having high specific strength, stiffness, and lightweight. However, these advanced materials are vulnerable to impact or other mechanical loadings especially thermosetting polymers due to their brittleness structure [1].

Self-healing in engineered materials such as polymeric composites can prevent catastrophic failures of composites by repairing minor internal damages [2]. Encapsulation of the healing agent within containers which are incorporated inside polymer matrix is one of the most useful approaches to develop self-healing materials. Fracture of containers leads to release healing agent into the cracks and undergoes a healing process [3–8]. Various types of the containers including microcapsules, microvascular networks, and hollow fibers are used in order to have an efficient healing system [6,9,10]. Self-healing approach based on microcapsule has significant disadvantages such as inadequate amount of healing agent for multiple healing and uncertainty of complete consumption of the healing agent and disruptive effect of microcapsule at high volume fraction on the orientation of reinforcing fibers [11,12]. Multiple healing could be achieved via another strategy of self-healing using tubular channels such as microvascular network and

hollow fibers due to the ability to contain a large amount of healing agent [6,13]. In the research work of Dry, healing material was used within hollow fibers in order to evaluate the healing possibility of polymer matrix composite [14]. Pang and Bond developed filled hollow fiber reinforced composite and managed to restore flexural strength of composite after impact damage [15]. In addition, Trask et al. showed that inclusion of self-healing multilayers hollow glass fibers into epoxy composites led to a considerable recovery of initial mechanical strength after a damage event [16,17]. Beside certain advantages of hollow fibers there are some drawbacks in their application such as mitigation of initial strength of the composite and the need of high stress to rupture the fibers at onset of the healing process [11,17].

Self-healing systems mentioned above have adverse effects on the mechanical properties of composite materials. Their existence as micro size containers in the composites would create stress concentrations which would trigger crack initiation [18]. Core-shell nanofibers have attracted attention of researchers due to having several orders of magnitude smaller diameters than the microcapsule and hollow fiber and minimum impact on polymer composite weight [19–25].

Coaxial electrospinning is a versatile method to produce core-shell nanofibers [26]. Wu et al. used coaxial electrospinning to encapsulate liquid dicyclopentadiene as the healing agent of epoxy resin into

\* Corresponding author.

E-mail address: [sborhani@cc.iut.ac.ir](mailto:sborhani@cc.iut.ac.ir) (S. Borhani).

**Table 1**  
Sample codes of the solutions.

Epoxy to PAN weight ratio	Sample code	PETMP to PAN weight ratio	Sample code
0.2	E0.2	0.2	P0.2
1	E1	1	P1
1.5	E1.5	1.5	P1.5

polyacrylonitrile (PAN) nanofibers to heal carbon fiber/epoxy composites [18]. Several research encapsulated resin and its cure inside nanofibers separately, where polymerization takes place into crack planes leading to the repair of the damaged area. Lee et al. fabricated self-healing polydimethylsiloxane composites including dimethylsiloxane resin and its curing agent into a PAN shell via coaxial electrospinning [21]. Another approach by this method was carried out by Neisiany et al. in which epoxy resin and amine were encapsulated into PAN nanofibers [6]. It is noticeable that the mentioned method requires four electrospinning instruments which makes the process complex and more difficult to control the parameters of electrospinning. Also, another problem of coaxial electrospinning is that the inner and outer polymer solution should be immiscible to obtain core-shell structure [27]. Core-shell nanofibers could also be produced via a single nozzle from either an emulsion or homogenous solutions [26]. Bazilevsky et al. already proposed the mechanism of emulsion electrospinning [28]. In homogenous solution electrospinning, phase separation and other kinetic and thermodynamic factors affect the morphology of the nanofibers [26]. Wei et al. showed that the composition ratio of polymer blend plays a critical role in the formation of core-shell structure [29]. Moreover, these works concluded that rapid solvent evaporation, the difference in solubility parameter of the compositions and viscosity of each material in solution could have a substantial effect on the formation of core-shell structure [27].

Epoxy resin is used in many fields such as transportation vehicles and wind turbine blade. Self-healing systems capable of healing damaged epoxy composites could increase the lifetime of the structural materials. At low temperatures, chemical reaction does not take place for most of the healing agents. This could be rectified by using a combination of epoxy and mercaptan and proper catalyst [30]. Core-shell nanofibers can be used as promising container to encapsulate healing agent. Based on our knowledge, encapsulation of two-component healing agents, epoxy resin and mercaptan in nanofibers has not been studied. Furthermore, due to the mentioned difficulties of coaxial electrospinning, the present study aims to fabricate core-shell nanofibers using the single nozzle accompanied by characterization and the potential use for self-healing application.

## 2. Experimental

### 2.1. Materials

PAN ( $M_w = 100000$  g/mol) was purchased from Polyacryl company which is a copolymer of acrylonitrile/vinyl acetate (95:5 by mol%). Epoxy resin (Araldite LY 5052-1) as the healing agent with the viscosity of 1 Pa s was obtained from Huntsman, Switzerland. Pentaerythritol tetrakis (3-mercaptopropionate) (PETMP) as the hardener of the epoxy resin with viscosity of 0.45 Pa s and density of 1280 kg/m<sup>3</sup> at 25 °C was obtained from Sigma-Aldrich, USA. N, N-dimethylbenzylamine (BDMA) as the catalyst and N, N-dimethylformamide (DMF) as the solvent were purchased from Merck, Germany.

### 2.2. Electrospinning

PAN solution with concentration of 12 wt%, was prepared by dissolving the exact amount of PAN powder in DMF under gentle stirring for 24 h at room temperature. In order to prepare polymer blend solution

of PAN-epoxy to produce core-shell nanofibers by a single nozzle, the epoxy resin was directly added to each PAN solution in a way that the weight ratio of the epoxy resin and PAN were 0.2, 1 and 1.5. Similar to the PAN-epoxy solutions, PETMP was added to prepared PAN solutions. The ultimate weight ratio of PAN-PETMP were 0.2, 1 and 1.5. Table 1 lists the prepared solutions of PAN-epoxy and PAN-PETMP and the sample code.

The viscosity of the solutions was measured using viscometer (Brookfield DV-II, USA). Prepared polymer blend solutions were electrospun from a single nozzle at ambient condition (24 °C and RH = 31%). The flow rate of the solutions was set between 0.125 and 0.135 ml/h and the applied voltage was 7 kV ± 0.5. Moreover, the distance between the nozzle to the collector was 13 cm.

## 2.3. Characterization

### 2.3.1. Fourier transform infrared spectroscopy (FTIR) analysis

FTIR spectra of electrospun nanofibers were performed using KBr pellets method by Bomem FTIR MB-series, MB-100 (Hartmann & Braun, Canada). The spectra were obtained in the wavenumber range of 3500–500 cm<sup>-1</sup> at room temperature. Thirty two scans were conducted in order to reduce the noise of the spectra.

### 2.3.2. Extraction of encapsulated materials

Extraction of the encapsulated materials was performed using methanol. First, the electrospun nanofibers were accurately weighed ( $W_i$ ). After crushing by sharp razor, the nanofibers were pressed and washed several times by methanol to eliminate the core content ( $W_{core}$ ) of the nanofibers. Finally, the dried electrospun nanofibers were weighed ( $W_{shell}$ ) to calculate the amount of encapsulated materials using equation (1) [31].

$$\% W_{core} = \left( 1 - \frac{W_s}{W_i} \right) \times 100 \quad (1)$$

### 2.3.3. Morphological characterization

Surface morphology of the electrospun nanofibers were observed by field emission scanning electron microscopy (FESEM) using Quanta FEG 450, USA. Also, the formation of core-shell nanofibers is confirmed by transmission electron microscopy (Philips CM30, Netherland) with 150 kV voltage.

### 2.3.4. Thermogravimetric analysis (TGA)

TGA experiments were performed under nitrogen atmosphere at a flow rate of 50 ml/min by Bahr STA 503, Germany. All samples (approximately 8 mg) were heated at a rate of 10 °C/min from room temperature to 700 °C. In order to eliminate the unencapsulated epoxy and PETMP, the surface of the nanofibers was washed by methanol.

### 2.3.5. Differential scanning calorimetry (DSC)

In order to study curing properties of the epoxy resin and PETMP in presence of BDMA, non-isothermal DSC was performed using Bahr DSC 302, Germany. The dynamic scans were made from 35 to 300 °C at a constant heating rate of 10 °C/min. Also, isothermal DSC was carried out at the constant temperature of 10 °C to study curing degree of the epoxy.

### 2.3.6. Mechanical testing

Tensile strength of PAN and hybrid nanofibers mats were conducted using Zwick 1446-60, Germany. Rectangular dimensions of the prepared samples were 3.5 × 1.5 cm and the grip to grip distance was set to 2.2 cm according to Sinha-Ray et al. [32]. Also the rate of stretching of 1 mm/min was set for all the tensile tests.

### 2.3.7. Nuclear magnetic resonance (NMR)

<sup>1</sup>H NMR and <sup>13</sup>C NMR were performed to obtain chemical structure of the epoxy resin using Bruker spectrometer operating at 400 MHz d6-

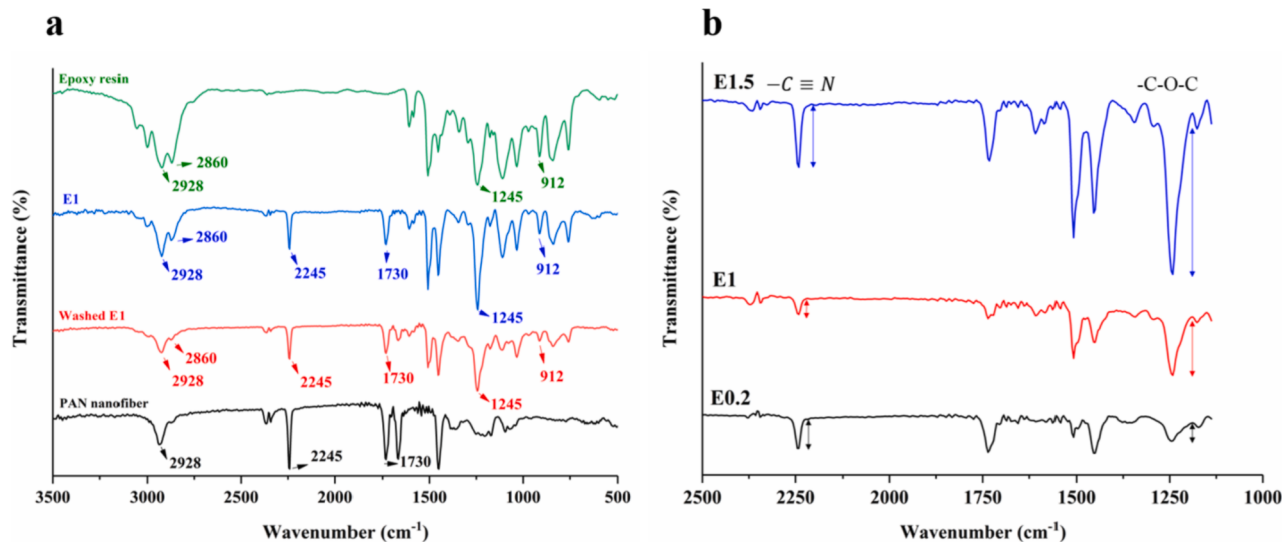


**Fig. 1.** (a) FTIR spectra of epoxy resin, PAN nanofibers and E1 nanofibers (washed and unwashed), (b) FTIR spectra of washed E0.2, E1 and E1.5 nanofibers.

**Table 2**

The peaks intensity of  $-C \equiv N$ ,  $-C-O-C$  and the ratio of peak intensity of  $-C-O-C$  to  $-C \equiv N$ .

Sample code	Peak intensity of $-C \equiv N$	Peak intensity of $-C-O-C$	Peak intensity ratio of $C-O-C$ to $C \equiv N$
E0.2	0.052	0.042	0.81
E1	0.026	0.106	4.08
E1.5	0.101	0.286	2.83

Acetone was used as solvent for the epoxy resin.

### 3. Results and discussion

#### 3.1. Chemical structure

FTIR spectroscopy was performed in order to study the chemical structure of electrospun nanofibers. Fig. 1a shows FTIR spectra of PAN nanofibers, epoxy resin and E1 nanofibers (unwashed/washed). The spectrum of PAN nanofiber exhibits a stretching absorption peaks of  $-C \equiv N$  and  $-C=O$  at 2245 cm<sup>-1</sup> and 1730 cm<sup>-1</sup>, respectively. For epoxy resin, the presence of  $-C-H$  band in aromatic and aliphatic ring of epoxy structure show two peaks of 2928 cm<sup>-1</sup> and 2860 cm<sup>-1</sup>, respectively. The bands at 1245 cm<sup>-1</sup> and 912 cm<sup>-1</sup> can be attributed to ether group ( $-C-O-C$ ) and oxirane group, respectively [6,7,33]. The unchanged characteristic peaks of PAN nanofiber and epoxy resin are

**Table 3**

The peaks intensity of  $-C \equiv N$ ,  $-SH$  and the ratio of peak intensity of  $-SH$  to  $-C \equiv N$ .

Sample code	Peak intensity of $-C \equiv N$	Peak intensity of $-SH$	Peak intensity ratio of $-SH$ to $-C \equiv N$
P0.2	0.058	0.017	0.29
P1	0.098	0.059	0.60
P1.5	0.150	0.054	0.36

also observed in unwashed E1 nanofiber spectrum, which is due to absence of chemical reaction between epoxy resin and PAN. These characteristic peaks are retained after washing the E1 nanofiber web by methanol which indicates that epoxy resin is well stored in the PAN nanofibers. Methanol washing has removed a slight amount of epoxy resin from the surfaces of the nanofibers, hence reducing the peaks intensity. Fig. 1b illustrates FTIR spectra of washed E0.2, E1 and E1.5 nanofibers in which the peak intensity can be used to estimate the loading content of epoxy resin. Table 2 shows the intensities of characteristic peaks of epoxy resin ( $-C-O-C$ ) and PAN ( $-C \equiv N$ ) and the peak intensity ratio. According to Table 2, the peak intensity ratio of E1 is more than E0.2 and E1.5 nanofibers. It seems that E1 nanofibers encapsulate more epoxy resin within it in comparison with two other samples.

For PETMP, its FTIR spectrum as illustrated in Fig. 2 exhibits stretching vibration peaks for  $C-H$  at 2956 cm<sup>-1</sup> and 2906 cm<sup>-1</sup> due

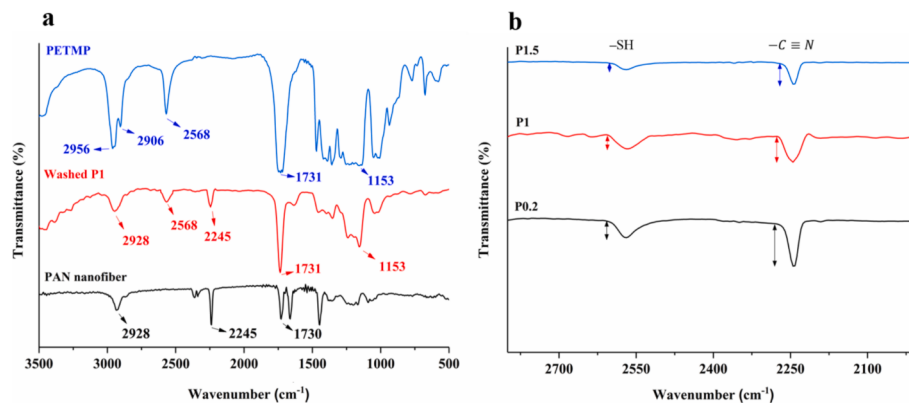


**Fig. 2.** (a) FTIR spectra of PETMP, PAN nanofiber and washed P1nanofibers, (b) FTIR spectra of washed P0.2, P1 and P1.5 nanofibers.

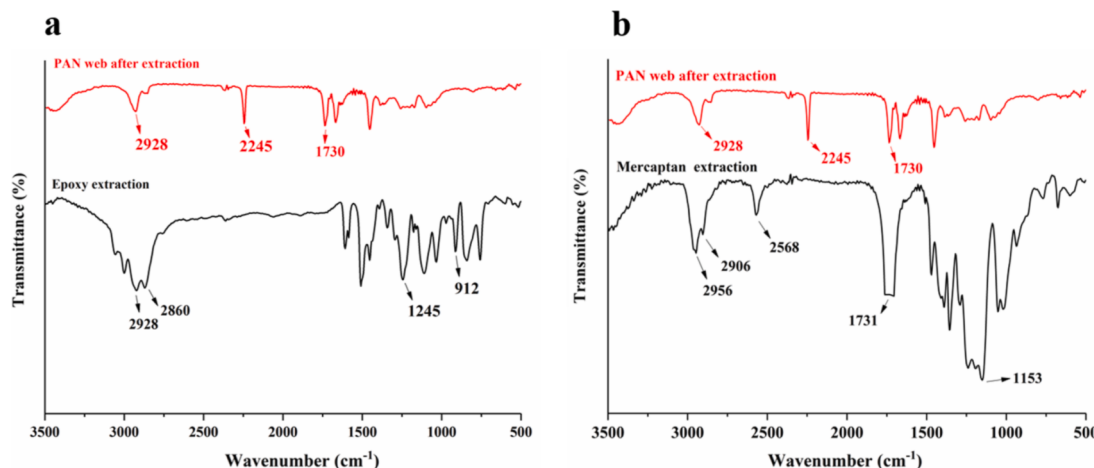


**Fig. 3.** (a) FTIR spectra of PAN nanofiber web and epoxy collected after extraction method, (b) FTIR spectra of PAN nanofiber web and PETMP obtained after extraction.

to the presence of  $-\text{CH}_2$  group, for  $-\text{SH}$  stretching at  $2568\text{ cm}^{-1}$ ,  $-\text{C}=\text{O}$  stretching at  $1731\text{ cm}^{-1}$  and stretching vibration of  $\text{C}-\text{O}$  at  $1153\text{ cm}^{-1}$  [34]. The characteristic peaks of PAN and PETMP are also observed in washed FTIR spectra of P1 nanofibers. These results indicate that PETMP are well encapsulated in PAN without any chemical reactions. According to Table 3, by measuring the peak intensity ratio of  $-\text{SH}$  to  $-\text{C}\equiv\text{N}$  using Omnic software, it was found that the P1 nanofibers contain more PETMP compared with P0.2 and P1.5 nanofibers. High amounts of healing materials lead to more efficient self-healing system. It can be concluded that E1 and P1 nanofibers are more appropriate samples for further analysis.

### 3.2. Extraction of core materials

The extraction method could verify the FTIR results obtained by using the characteristic peaks intensity of core materials and PAN. According to extraction results, the loading content of epoxy resin in 3 samples of E0.2, E1 and E1.5 nanofibers are 7 wt%, 19 wt% and 9 wt%, respectively. Also, the loading content of PETMP in P0.2, P1 and P1.5 nanofibers are 10.4 wt%, 25.7 wt% and 17.7 wt%, respectively which are in accordance with FTIR results. The validity of extraction method could be confirmed with FTIR analysis. According to Fig. 3, the FTIR spectra of nanofibers show only the PAN characteristic peaks and the extracted core materials show only their related peaks (epoxy resin or PETMP).

### 3.3. Morphological characterization of electrospun nanofibers

Fig. 4 exhibits FESEM images of the electrospun nanofibers along with their corresponding diameter distributions which were measured using Digimizer software. The nanofibers are uniform without formation of beads. Maximum average diameter for encapsulated epoxy and PETMP nanofibers are related to E1 and P1 nanofibers with average diameter of 643 nm (d) and 455 nm (e), respectively.

Higher average diameter of the nanofibers containing epoxy when compared with those containing PETMP at the same core to PAN weight ratio is due to increasing viscosity of the solutions [35]. Viscosity of the solutions for 12 wt% PAN, E1 and P1 are 840, 965 and 870 cP, respectively. In addition, the viscosity of E0.2 and E1.5 are 855 and 1100 cP and viscosity of P0.2 and P1.5 are 848 and 950 cP, respectively. Also, cores diameter of nanofibers may have significant impact on nanofibers diameter which has been studied by TEM images of electrospun nanofibers.

In order to verify formation of core-shell structure produced by single nozzle electrospinning, TEM images of encapsulated PAN, epoxy

and PETMP nanofibers were obtained. According to Fig. 5, the epoxy and PETMP are uniformly located at the centre of the nanofibers and maximum ratio of core to fiber diameter related to E1 and P1 nanofibers are 0.69 and 0.61, respectively. According to Fig. 5b, E0.2 nanofibers would solid and core-shell structures have been formed and this could be the reason for having minimum loading content of epoxy.

### 3.4. Thermogravimetric analysis

TGA is conducted in order to study the thermal stability of core-shell nanofibers. Also, due to increasing temperature during TGA analysis, the weight change of core-shell nanofibers could be used to calculate the amount of epoxy resin and PETMP stored in electrospun nanofibers. Fig. 6a shows the TGA plots for PAN nanofibers, epoxy resin and washed and unwashed E1 nanofibers. In the case of PAN nanofibers, the curve shows three weight loss ranges. Evaporation of moisture and residual DMF took place at  $100\text{--}150\text{ }^\circ\text{C}$ , escaping the volatile substances such as ammonia, hydrogen cyanide, and acetonitrile at  $300\text{--}350\text{ }^\circ\text{C}$  and degradation of PAN basis at  $380\text{--}500\text{ }^\circ\text{C}$ . For epoxy resin, the thermal degradation takes place at  $200\text{--}500\text{ }^\circ\text{C}$  producing phenolic compounds [6]. The TGA data for unwashed E1 nanofibers shows thermal degradation at  $250\text{--}300\text{ }^\circ\text{C}$ . This degradation has happened with gentle slope for washed E1 nanofibers due to elimination of epoxy resin from the surface of nanofibers. In unwashed E1 nanofibers, degradation of PAN and epoxy occur simultaneously, while in washed E1 nanofibers, degradation of PAN happens prior to epoxy resin. The difference between weight loss of PAN nanofibers and the core-shell nanofibers at  $500\text{ }^\circ\text{C}$  could approximately determine the amount of epoxy resin encapsulated into nanofibers. According to Fig. 6a, the epoxy content of unwashed and washed core-shell nanofibers are 21 wt% and 16 wt%, respectively, hence 5 wt% difference of epoxy content shows that there was a slight unencapsulated epoxy on the surface of nanofibers.

Fig. 6b shows the TGA results for PETMP encapsulated nanofibers. The onset of degradation starts at  $250\text{ }^\circ\text{C}$ . Highest rates of degradation has occurred at  $360\text{ }^\circ\text{C}$  and  $436\text{ }^\circ\text{C}$ . In these temperatures, the products such as hydrogen sulfide, carbon dioxide and saturated/unsaturated hydrocarbons have been produced during decomposition of PETMP [34]. Fig. 6b also shows that the thermal degradation of washed P1 nanofibers starts from decomposition of PAN shell and the maximum weight loss occurs around  $350\text{ }^\circ\text{C}$  where the released PETMP is degraded. The TGA data for unwashed P1 nanofibers indicated that the amount of unencapsulated PETMP is not significant. The PETMP content of unwashed and washed P1 nanofibers were around 24.4 wt% and 23 wt%, respectively.

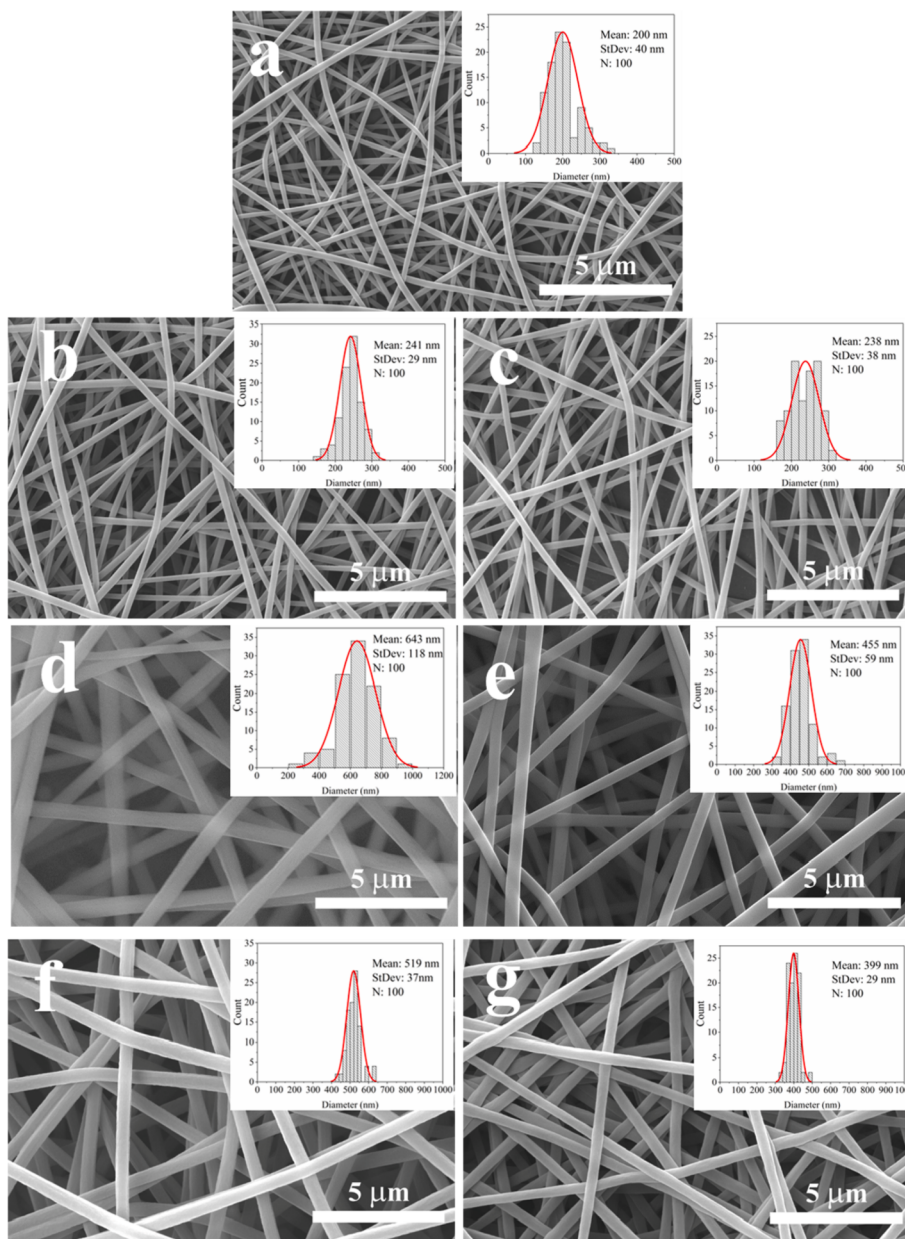


**Fig. 4.** FESEM images of electrospun nanofibers along with their corresponding diameter distributions (a) PAN nanofibers, (b) E0.2 nanofibers, (c) P0.2 nanofibers, (d) E1 nanofibers, (e) P1 nanofibers, (f) E1.5 nanofibers, (g) P1.5 nanofibers.

### 3.5. Epoxy-mercaptop interaction

In order to elucidate the self-healing interaction of epoxy and PETMP encapsulated in PAN nanofibers, the tertiary amine catalyst (BDMA) was added to P1 solution (BDMA: PETMP 1:10 wt%). Hybrid nanofiber mat was produced by electrospinning of two types of core-shell nanofibers (E1 and P1/BDMA) on the same substrate. Fig. 7a shows SEM image of damaged PAN nanofiber mat, while Fig. 7b shows damaged hybrid mat that has been repaired by reaction between epoxy, PETMP and its catalyst. It should be noted that the hybrid nanofibers were first washed by methanol to eliminate the unencapsulated materials.

DSC analysis were performed with the aim of monitoring the self-healing process of the system. DSC curve of PAN nanofiber in Fig. 8a shows an exothermic peak at approximately 275 °C which is due to cyclization of PAN [6]. Fig. 8b shows the DSC plot of the model mixture of epoxy, PETMP and BDMA as healing system. Curing of epoxy resin with PETMP and BDMA has shown an exothermic peak centered at

about 69 °C [30]. This exothermic peak also has been observed in the DSC plot of damaged hybrid nanofibers mat (Fig. 8c). For undamaged hybrid nanofibers mat before washing, according to Fig. 8d, three peaks were observed between approximately 60 to 130 °C that show gradual release of the self-healing materials. The peak centered at 69 °C is due to the reaction of the materials located on the surface of nanofibers which did not appear in the washed undamaged hybrid nanofibers mat (Fig. 8e).

The isothermal DSC curve is carried out at 10 °C in order to study curing degree of epoxy resin at subroom temperature. Therefore, damaged hybrid nanofibers mat was placed in the DSC pan and immediately tested. Fig. 9a shows that within 200 min the epoxy is cured. The degree of cure ( $\alpha$ ) is approximately about 0.7 according to Fig. 9b which has been extracted by equations (2)–(4) as follows [36]:

$$H_R = \int_0^{t_f} \left( \frac{dQ}{dt} \right) dt \quad (2)$$

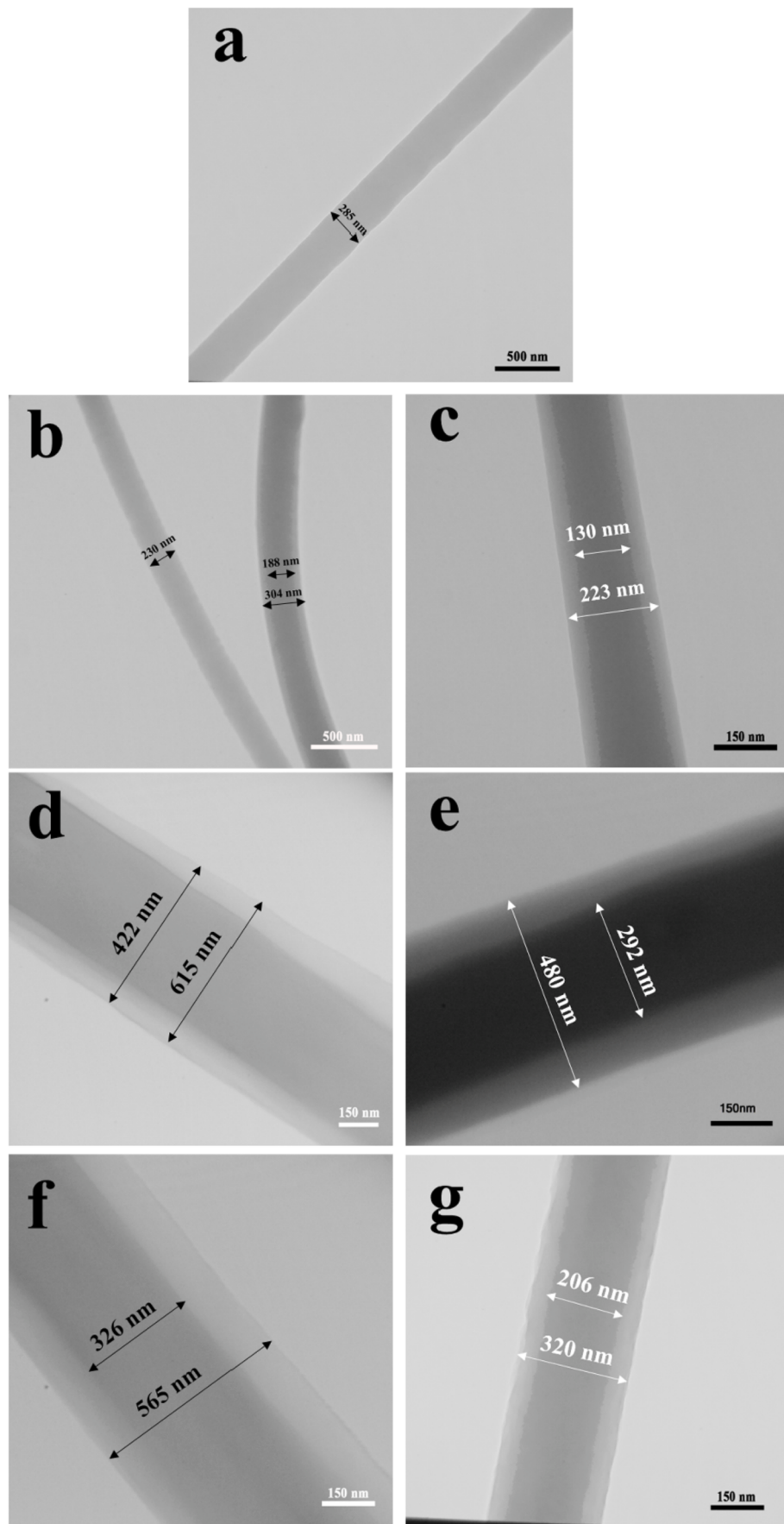


**Fig. 5.** TEM images of core-shell nanofibers (a) PAN nanofiber, (b) E0.2 nanofibers, (c) P0.2 nanofiber, (d) E1 nanofiber, (e) P1 nanofiber, (f) E1.5 nanofiber, (g) P1.5 nanofiber.

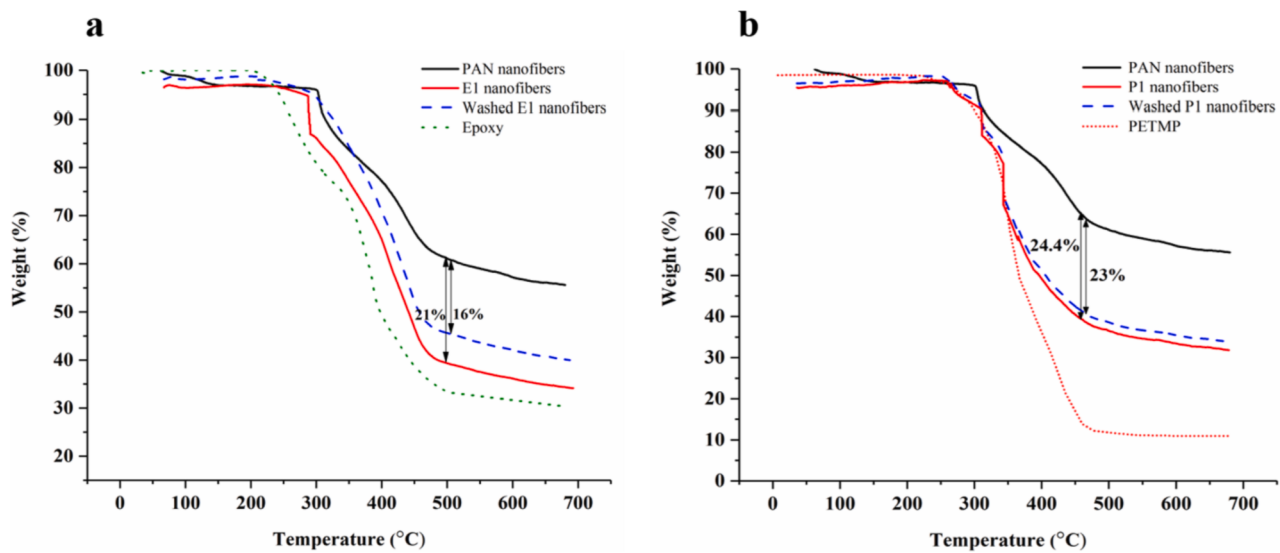


**Fig. 6.** (a) TGA curve of PAN nanofibers, epoxy resin and washed and unwashed E1 nanofibers, (b) TGA curve of PAN nanofibers, PETMP and washed and unwashed P1 nanofibers.

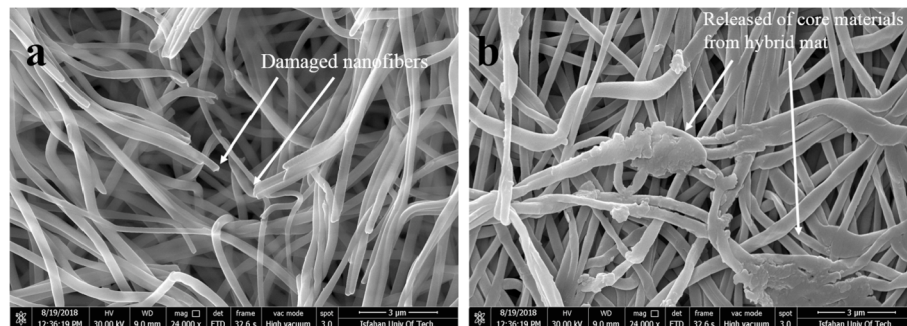


**Fig. 7.** FESEM images (a) damaged PAN nanofibers mat, (b) damaged hybrid nanofibers mat that has been repaired by reaction between epoxy, PETMP and its catalyst.

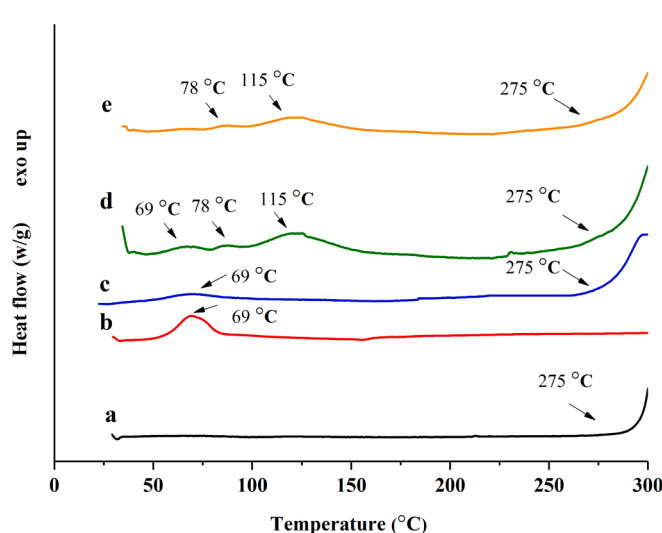


**Fig. 8.** Nonisothermal DSC plot (a) PAN nanofibers mat, (b) mixture of epoxy, PETMP and BDMA, (c) washed damaged hybrid nanofibers mat, (d) unwashed undamaged hybrid nanofibers mat., (e) Washed undamaged hybrid nanofibers mat.

$$H = \int_0^t \left( \frac{dQ}{dt} \right) dt \quad (3)$$

$$\alpha = \frac{H}{H_R} \quad (4)$$

where  $t_f$  is total reaction time and  $H_R$  and  $H$  are the heat of complete reaction and the partial reaction at a time  $t$ , respectively.

Self-healing interaction were also studied by mechanical properties of electrospun nanofibers. Fig. 10 shows stress-strain curves of PAN and hybrid nanofiber mats at 10 °C. The thickness of PAN and hybrid mats were 25 and 60 µm, respectively. According to Fig. 10, the Young's modulus of PAN and hybrid nanofiber mats were 28.5 and 32.1 MPa, respectively. It was expected that the solid PAN mat have higher Young's modulus compared to hybrid mat. But the chemical reaction of unencapsulated epoxy and PETMP on the surface of the hybrid nanofibers could lead to surface adhesion and consequently increased the modulus of hybrid nanofibers.

The ultimate tensile stress of PAN nanofibers was more than the hybrid nanofibers. This could be related to solid formation of PAN nanofibers in comparison with the core-shell structure of hybrid nanofibers. Also, according to Fig. 4a, PAN nanofibers had lower average diameter which increased the ultimate tensile stress [37,38].

Stress-strain curve of electrospun nanofibers have 3 regions of elastic, plastic and catastrophic failure [21]. Fig. 11 (a, b) shows the results of the repeated tensile stress of PAN and hybrid mats up to a

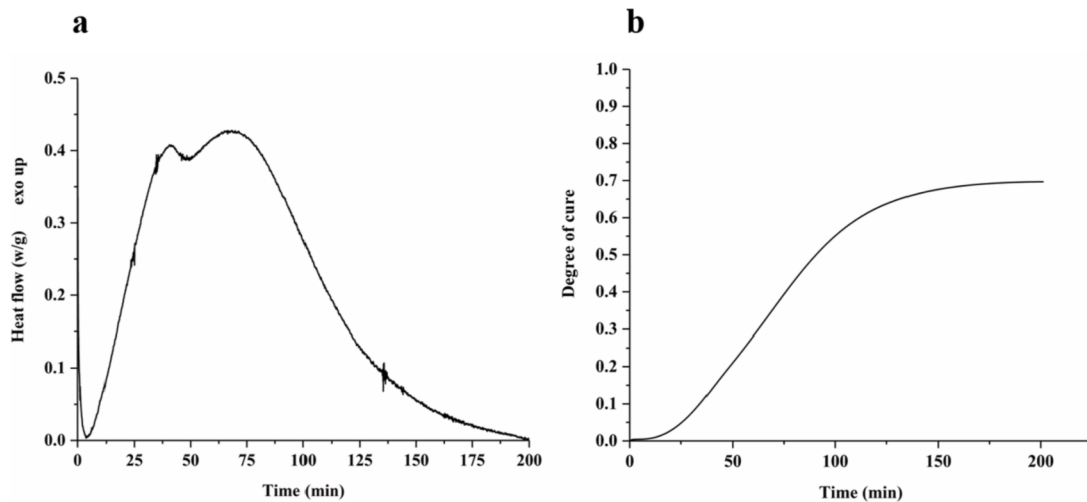


**Fig. 9.** (a) Isothermal DSC plot of damaged hybrid nanofibers mat at 10 °C, (b) curing degree of epoxy resin at 10 °C.

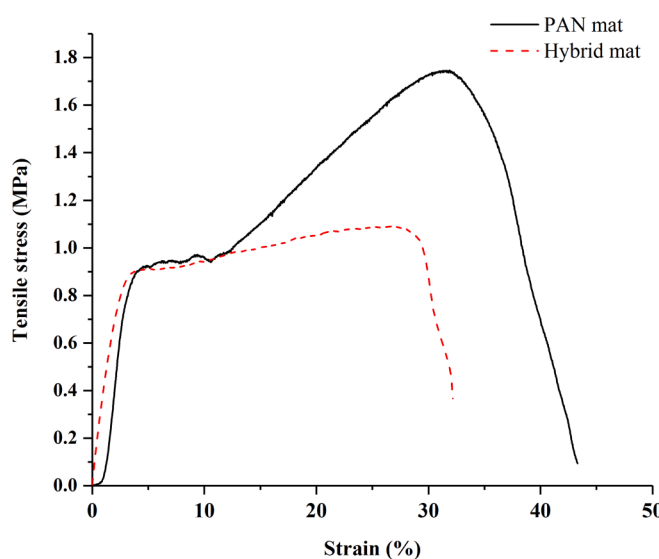


**Fig. 10.** Stress-strain curves of PAN and hybrid mats at 10 °C.

strain of 10% where the samples were in the initial part of plastic region. After each repeat, the samples were kept in temperature control chamber for 200 min at 10 °C according to result of isothermal DSC in Fig. 9. The tensile test were performed immediately after removing the samples from the chamber. According to Fig. 11 (a, b), while PAN mat strength reduced more than 80%, the hybrid mat only decreased by 13%. These results indicates that the releasing and subsequent curing of the core materials had hindered tensile strength reduction.

Similar tests were performed except that the electrospun nanofibers were stretched to a strain of 25% where the samples were near the catastrophic failure. Fig. 11 (c, d) shows that releasing of epoxy resin and PETMP had no effect on tensile strength. Therefore the tensile strength of PAN and hybrid mats were reduced entirely after three times stretching.

### 3.6. Mechanism of core-shell nanofibers

Due to the polar nature of DMF, epoxy and PETMP, emulsion electrospinning could not be the mechanism governing the formation of core-shell nanofibers [39]. Phase separation is another possible mechanism that could control the formation of core-shell structure by single nozzle [26]. In order to study the phase separation of PAN-Epoxy, the

Hansen solubility parameters ( $\delta_d$ ,  $\delta_p$ ,  $\delta_h$ ) of epoxy is calculated using Hoftyzer- Van Krevelen method as follows [40]:

$$\delta_d = \frac{\sum F_{di}}{V} \quad (5)$$

$$\delta_p = \sqrt{\frac{\sum F_{pi}^2}{V}} \quad (6)$$

$$\delta_h = \sqrt{\frac{\sum E_{hi}}{V}} \quad (7)$$

where  $F_{di}$ ,  $F_{pi}$  and  $E_{hi}$  are the group contribution to the dispersion forces, polar forces and hydrogen bonding energy, respectively. Also, i refers to structural group in molecule and V is the molar volume [40]. To figure out the chemical structure of epoxy resin, <sup>1</sup>H NMR and <sup>13</sup>C NMR are used. As demonstrated in Fig. 12, which shows <sup>1</sup>H NMR of epoxy resin (Araldite LY 5052), the structural groups could be obtained from the corresponding peaks. Aromatic protons appear in the range of 6.9–7.2 ppm. Also the peaks in the range of 2.5–4.5 ppm refer to protons of epoxide group [41,42]. Fig. 13 illustrates <sup>13</sup>C NMR of epoxy resin. The aromatic carbons are in the range of 114–140 ppm and the peaks around 70 and 72 ppm are related to the methylene group attached to oxygen [43].

According to results of NMR study, the proposed epoxy structure (Fig. 14) is used for calculating solubility parameter of epoxy resin. Due to the constant values of Krevelen and Hoftyzer method for the position of any substitution on benzene, the epoxy phenol structure has to be simplified [40].

For the structures shown above, data used for calculation of Hansen solubility parameters of epoxy resin are presented in Table 4 and Table 5.

The molar volume of epoxy novolac and 1, 4 Butanediol diglycidyl ether are 132 and 183 cm<sup>3</sup>/mol, respectively. The calculated solubility parameters of epoxy resin are shown in Table 6.

The immiscibility of PAN and epoxy resin is confirmed through the value of  $\Delta\bar{\delta}$  as follows [45]:

$$\Delta\bar{\delta} = [(\delta_{d2} - \delta_{d1})^2 + (\delta_{p2} - \delta_{p1})^2 + (\delta_{h2} - \delta_{h1})^2]^{0.5} \quad (8)$$

According to Krevelen et al., two compounds are miscible when  $\Delta\bar{\delta} \leq 5 \text{ MPa}^{0.5}$ , while the current PAN-epoxy system is 11.83 MPa<sup>0.5</sup> which is considerably higher than the threshold [45]. Therefore, PAN and epoxy resin opted to separate into two phases due to evaporation of DMF during electrospinning and the PAN-epoxy core-shell nanofibers have been resulted.

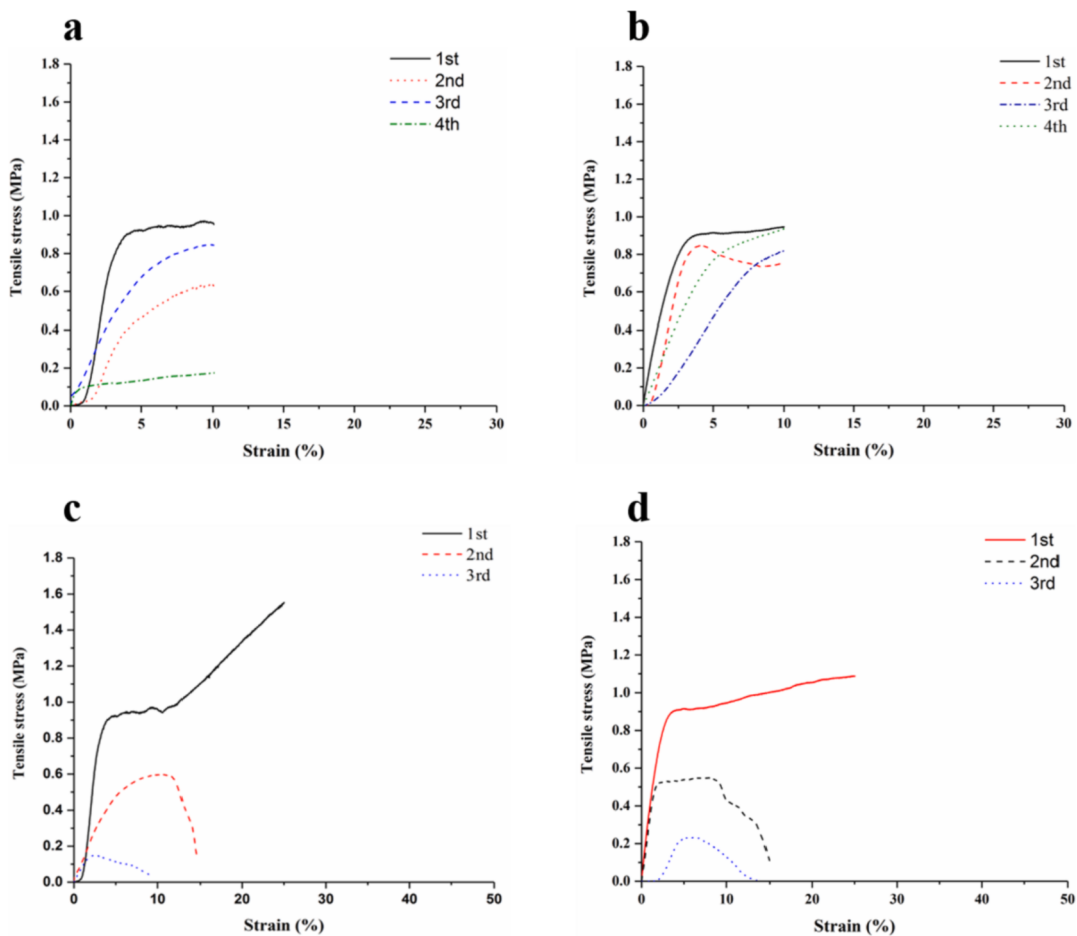


**Fig. 11.** Stress-strain curves of PAN and hybrid mats at 10 °C, (a) Strain: 10%, sample: PAN mat, (b) Strain: 10%, sample: hybrid mat, (c) Strain: 25%, sample: PAN mat, (d) Strain: 25%, sample: hybrid mat.

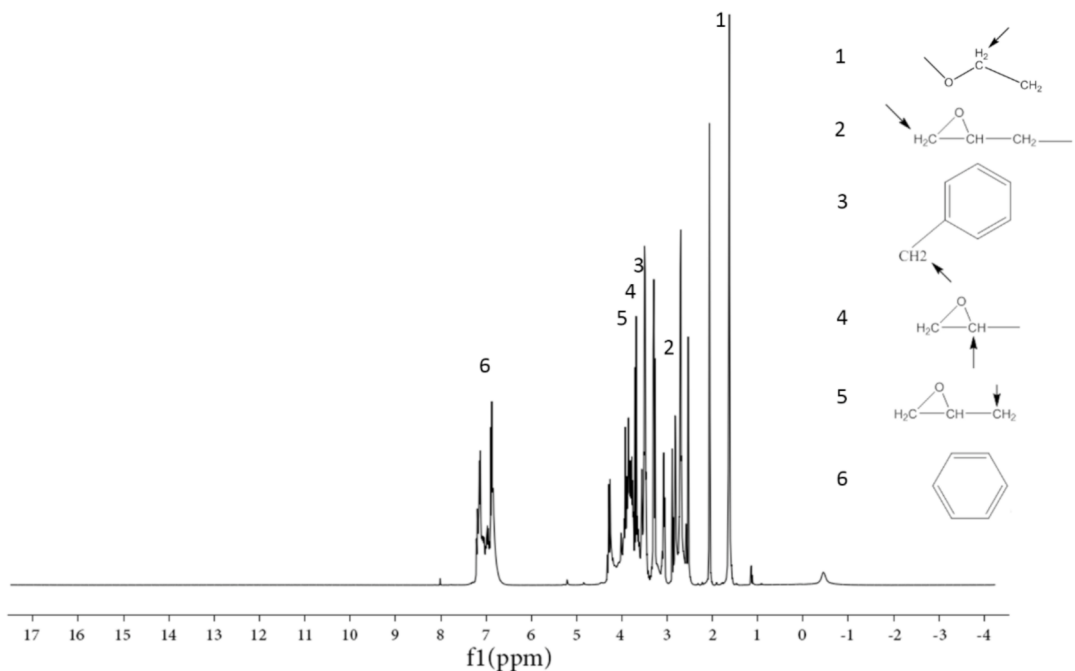


**Fig. 12.** <sup>1</sup>H NMR spectra of epoxy resin (<sup>6</sup>d-acetone, 400 MHz).

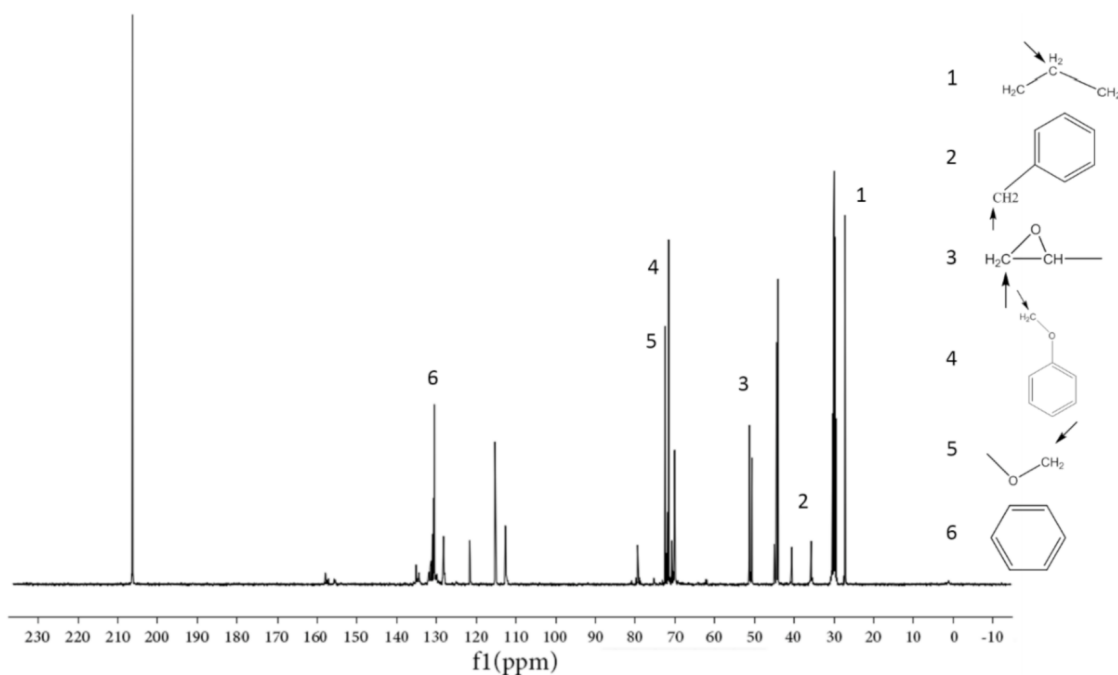
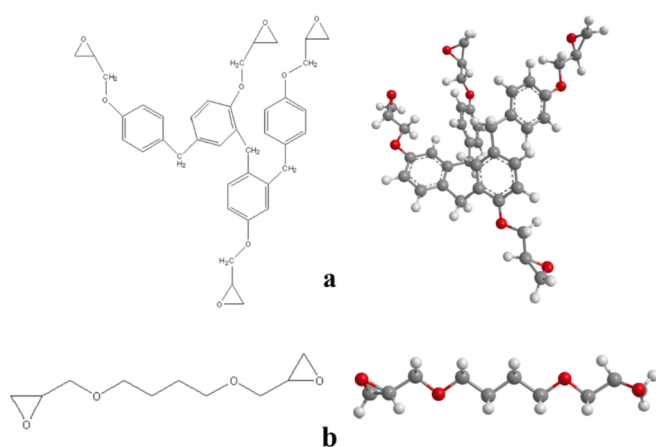
Fig. 13.  $^{13}\text{C}$  NMR spectra of epoxy resin (d<sub>6</sub>-acetone, 400 MHz).

Fig. 14. 2D and 3D structure of epoxy resin (a) epoxy phenol novolak, (b) 1, 4-butanediol diglycidyl ether.

The Hoftzyer-Krevelen method is not suitable for determining miscibility of PAN-PETMP due to lack of values for -SH group. Therefore, the Hildebrand solubility parameter was used for the mentioned compounds. Flory-Huggins interaction parameter was calculated as follows [26]:

$$\delta = \frac{\rho(\sum F)}{M} \quad (9)$$

$$\chi_{12} = \frac{V_i}{RT} (\delta_1 - \delta_2)^2 \quad (10)$$

where  $\delta$  is the Hildebrand solubility parameter,  $\rho$  is the density and  $M$  is the molecular weight and  $F$  is the molar attraction constant. For polymer,  $\rho$  and  $M$  are the density of PAN and molecular weight of PAN segment, respectively. Also,  $\chi_{12}$  is the Flory-Huggins interaction parameter,  $V_i$  is molar volume of PETMP,  $R$  is the gas constant,  $T$  is the absolute temperature and  $\delta_1$  and  $\delta_2$  are the Hildebrand solubility parameters of PAN and PETMP, respectively [26]. Table 7 shows molar attraction constant of group structures at 25 °C [46].

According to Table 7 the Hildebrand solubility parameter of PAN and PETMP are calculated 25.7 and 21.9 Mpa<sup>0.5</sup>, respectively. Therefore, the

Table 5

Solubility parameter component group contributions for 1, 4 butanediol diglycidyl ether [40].

Group	Frequency	$F_{di} \left( \frac{MJ}{m^3} \right)^{0.5} \cdot mol^{-1}$	$F_{pi} \left( \frac{MJ}{m^3} \right)^{0.5} \cdot mol^{-1}$	$E_{hi} J \cdot mol^{-1}$
CH <sub>2</sub>	8	270	0	0
>CH-	2	80	0	0
-O-	4	100	400	3000
Ring	2	190	0	0

Table 4

Solubility parameter component group contributions for epoxy phenol novolac [40].

Group	Frequency	$F_{di} \left( \frac{MJ}{m^3} \right)^{0.5} \cdot mol^{-1}$	$F_{pi} \left( \frac{MJ}{m^3} \right)^{0.5} \cdot mol^{-1}$	$E_{hi} J \cdot mol^{-1}$
CH <sub>2</sub>	2	270	0	0
>CH-	1	80	0	0
-O-	1	1270	110	0
-O-Ring	2	100	400	3000
	1	190	0	0

**Table 6**  
Solubility parameter of PAN, DMF and epoxy resin.

Compound	$\delta_d \text{ MPa}^{0.5}$	$\delta_p \text{ MPa}^{0.5}$	$\delta_h \text{ MPa}^{0.5}$	$\delta_t \text{ MPa}^{0.5}$
PAN [44]	18.2	16.2	6.8	25.3
DMF [44]	17.4	13.7	11.3	24.8
Epoxy phenol Novolac	17.3	4.4	6.7	19
1,4-Butanediol diglycidyl ether	16.9	4.4	8.1	19.2
Epoxy resin	17.1	4.4	7.1	19

**Table 7**  
Molar attraction constants at 25 °C [46].

Group	Molar attraction F cal <sup>1/2</sup> cm <sup>3/2</sup>
CH <sub>3</sub>	214
CH <sub>2</sub>	133
CH	28
CN	410
C (single-bonded)	-93
COO	310
SH	315

Flory-Huggins interaction parameter of PAN-PETMP is calculated to be 2.21 which is higher than threshold (0.5) and PAN and PETMP are significantly immiscible. According to theoretical results, it could be concluded that the core-shell nanofibers were produced due to the immiscibility of PAN-PETMP.

Theoretical results showed that PAN-epoxy and PAN-PETMP were immiscible. However, the electrospinning solutions should be homogeneous during electrospinning. Fig. 15 shows the photographs of the PAN, PAN-epoxy and PAN-PETMP solutions during 3 days. According to Fig. 15, different solutions were in the stability form and no phase separation has occurred.

In fact, evaporation of DMF during electrospinning led to phase separation of PAN-epoxy and PAN-PETMP which has occurred simultaneously with core-shell nanofibers formation. In order to clarify the effect of DMF evaporation on stability of the solutions, one droplet of

each solution was dropped on a microscope slide. According to Fig. 16 all the droplets were initially homogenous. After a while, by evaporation of DMF, PAN became solid and no phase separation was observed in the PAN solution. In contrast, the observation of the liquid droplets (epoxy or PETMP) in the solid substrate (PAN), confirmed by FTIR, indicated that the phase separation of PAN-epoxy and PAN-PETMP solutions were taken place during solvent evaporation. Therefore, theoretical calculations and experimental results confirmed the formation of core-shell nanofibers during electrospinning.

#### 4. Conclusions

Hybrid core-shell nanofibers mat containing epoxy resin and mercaptan were fabricated using single nozzle electrospinning. The extraction results showed that the highest loading content of epoxy resin and mercaptan were obtained at epoxy (or mercaptan) to PAN weight ratio of 1. The highest loading content of epoxy resin and mercaptan were 19.0 wt% and 25.7 wt%, respectively. FTIR results confirmed absence of any chemical reaction between the cores and shell materials. FESEM images illustrated that the electrospun nanofibers are uniform without beads. In addition, TEM images showed core-shell formation structure of electrospun nanofibers. Mechanical properties of hybrid mats indicated that the releasing and subsequent curing of the core materials led to hinder tensile strength reduction. Immiscibility of two substances plays a major role in the formation of core-shell structure. By calculating solubility parameters of PAN, epoxy resin and mercaptan, it can be concluded that the epoxy and mercaptan are immiscible with PAN. TGA and nonisothermal DSC analysis showed that epoxy and mercaptan are encapsulated into nanofibers. Moreover, curing degree of epoxy resin at 10 °C was 0.7, showing that the self-healing system used in this study could be suitable in cold weather condition.

#### Funding

This research did not receive any specific grant from funding agencies in the public, commercial, or not-for-profit sectors.



Fig. 15. Photographs of PAN, PAN-epoxy and PAN-PETMP solutions during 3 days.

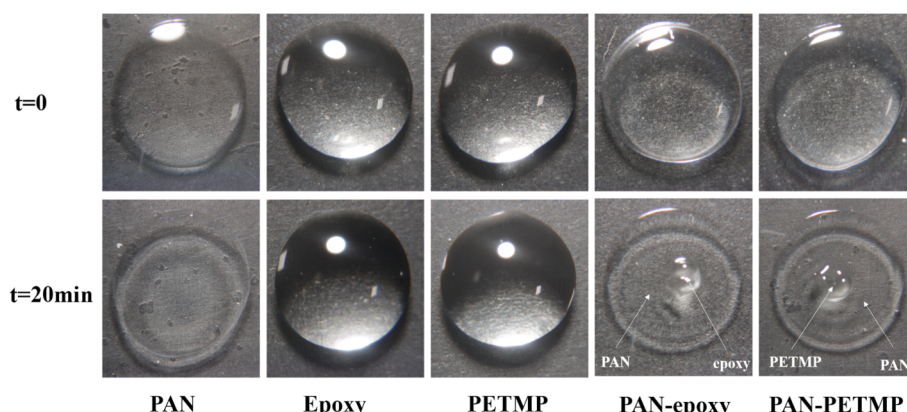


Fig. 16. Photographs of one droplet of PAN, PAN-epoxy, PAN-PETMP solutions and epoxy and PETMP.

## Declaration of competing interest

The authors declare that they have no known competing financial interests or personal relationships that could have appeared to influence the work reported in this paper.

## References

- [1] G. Li, Self-healing Composites: Shape Memory Polymer Based Structures, John Wiley & Sons, 2014.
- [2] M.W. Lee, S. An, H.S. Jo, S.S. Yoon, A.L. Yarin, Self-healing nanofiber-reinforced polymer composites. 2. Delamination/debonding and adhesive and cohesive properties, *ACS Appl. Mater. Interfaces* 7 (35) (2015) 19555–19561.
- [3] S.R. White, N. Sottos, P. Geubelle, J. Moore, M.R. Kessler, S. Sriram, E. Brown, S. Viswanathan, Autonomic healing of polymer composites, *Nature* 409 (6822) (2001) 794.
- [4] H. Jin, G.M. Miller, N.R. Sottos, S.R. White, Fracture and fatigue response of a self-healing epoxy adhesive, *Polymer* 52 (7) (2011) 1628–1634.
- [5] F. Ahangaran, M. Hayaty, A.H. Navarchian, Morphological study of polymethyl methacrylate microcapsules filled with self-healing agents, *Appl. Surf. Sci.* 399 (2017) 721–731.
- [6] R.E. Neisiany, S.N. Khorasani, J.K.Y. Lee, S. Ramakrishna, Encapsulation of epoxy and amine curing agent in PAN nanofibers by coaxial electrospinning for self-healing purposes, *RSC Adv.* 6 (74) (2016) 70056–70063.
- [7] F. Ahangaran, A.H. Navarchian, M. Hayaty, K. Esmailpour, Effect of mixing mode and emulsifying agents on micro/nanoencapsulation of low viscosity self-healing agents in polymethyl methacrylate shell, *Smart Mater. Struct.* 25 (9) (2016), 095035.
- [8] H.P. Wang, Y.C. Yuan, M.Z. Rong, M.Q. Zhang, Self-healing of thermoplastics via living polymerization, *Macromolecules* 43 (2) (2009) 595–598.
- [9] J.H. Park, P.V. Braun, Coaxial electrospinning of self-healing coatings, *Adv. Mater.* 22 (4) (2010) 496–499.
- [10] W. Ballout, A. Périchaud, L. Caserta, M. Devassine, C.L. Nistor, R. Iskakov, Encapsulation methods for photo-polymerisable self-healing formulations, *J. Microencapsul.* 33 (4) (2016) 331–343.
- [11] S.K. Ghosh, Self-healing Materials: Fundamentals, Design Strategies, and Applications, John Wiley & Sons, 2009.
- [12] J.-P. Pascault, R.J. Williams, Epoxy Polymers: New Materials and Innovations, John Wiley & Sons, 2009.
- [13] Q. Li, N.H. Kim, D. Hui, J.H. Lee, Effects of dual component microcapsules of resin and curing agent on the self-healing efficiency of epoxy, *Compos. B Eng.* 55 (2013) 79–85.
- [14] C. Dry, Procedures developed for self-repair of polymer matrix composite materials, *Compos. Struct.* 35 (3) (1996) 263–269.
- [15] J.W. Pang, I.P. Bond, A hollow fibre reinforced polymer composite encompassing self-healing and enhanced damage visibility, *Compos. Sci. Technol.* 65 (11–12) (2005) 1791–1799.
- [16] R. Trask, I. Bond, Biomimetic self-healing of advanced composite structures using hollow glass fibres, *Smart Mater. Struct.* 15 (3) (2006) 704.
- [17] R. Trask, G. Williams, I. Bond, Bioinspired self-healing of advanced composite structures using hollow glass fibres, *J. R. Soc. Interface* 4 (13) (2007) 363–371.
- [18] X.F. Wu, A. Rahman, Z. Zhou, D.D. Pelot, S. Sinha-Ray, B. Chen, S. Payne, A. L. Yarin, Electrospinning core-shell nanofibers for interfacial toughening and self-healing of carbon-fiber/epoxy composites, *J. Appl. Polym. Sci.* 129 (3) (2013) 1383–1393.
- [19] M.W. Lee, S. An, C. Lee, M. Liou, A.L. Yarin, S.S. Yoon, Hybrid self-healing matrix using core–shell nanofibers and capsuleless microdroplets, *ACS Appl. Mater. Interfaces* 6 (13) (2014) 10461–10468.
- [20] S. An, M. Liou, K.Y. Song, H.S. Jo, M.W. Lee, S.S. Al-Deyab, A.L. Yarin, S.S. Yoon, Highly flexible transparent self-healing composite based on electrospun core–shell nanofibers produced by coaxial electrospinning for anti-corrosion and electrical insulation, *Nanoscale* 7 (42) (2015) 17778–17785.
- [21] M.W. Lee, S. An, H.S. Jo, S.S. Yoon, A.L. Yarin, Self-healing nanofiber-reinforced polymer composites. 1. Tensile testing and recovery of mechanical properties, *ACS Appl. Mater. Interfaces* 7 (35) (2015) 19546–19554.
- [22] J.S.M. Zanjani, B.S. Okan, I. Letofsky-Papst, Y. Menceloglu, M. Yildiz, Repeated self-healing of nano and micro scale cracks in epoxy based composites by tri-axial electrospun fibers including different healing agents, *RSC Adv.* 5 (89) (2015) 73133–73145.
- [23] M.W. Lee, S.S. Yoon, A.L. Yarin, Solution-blown core–shell self-healing nano- and microfibers, *ACS Appl. Mater. Interfaces* 8 (7) (2016) 4955–4962.
- [24] M.W. Lee, S. Sett, S.S. Yoon, A.L. Yarin, Fatigue of self-healing nanofiber-based composites: static test and subcritical crack propagation, *ACS Appl. Mater. Interfaces* 8 (28) (2016) 18462–18470.
- [25] M.W. Lee, S. Sett, S.S. Yoon, A.L. Yarin, Self-healing of nanofiber-based composites in the course of stretching, *Polymer* 103 (2016) 180–188.
- [26] J.-F. Zhang, D.-Z. Yang, F. Xu, Z.-P. Zhang, R.-X. Yin, J. Nie, Electrospun core–shell structure nanofibers from homogeneous solution of poly (ethylene oxide)/chitosan, *Macromolecules* 42 (14) (2009) 5278–5284.
- [27] M. Wei, B. Kang, C. Sung, J. Mead, Core-sheath structure in electrospun nanofibers from polymer blends, *Macromol. Mater. Eng.* 291 (11) (2006) 1307–1314.
- [28] A.V. Bazilevsky, A.L. Yarin, C.M. Megaridis, Co-electrospinning of core–shell fibers using a single-nozzle technique, *Langmuir* 23 (5) (2007) 2311–2314.
- [29] M. Wei, B. Kang, C. Sung, J. Mead, Preparation of Nanofibers with Controlled Phase Morphology from Electrospinning of Polybutadiene-Polycarbonate Blends, ACS Publications, 2006, pp. 149–162. Chapter 11.
- [30] Y.C. Yuan, M.Z. Rong, M.Q. Zhang, J. Chen, G.C. Yang, X.M. Li, Self-healing polymeric materials using epoxy/mercaptan as the healant, *Macromolecules* 41 (14) (2008) 5197–5202.
- [31] Q. Li, A.K. Mishra, N.H. Kim, T. Kuila, K.-t. Lau, J.H. Lee, Effects of processing conditions of poly(methylmethacrylate) encapsulated liquid curing agent on the properties of self-healing composites, *Compos. B Eng.* 49 (2013) 6–15.
- [32] S. Sinha-Ray, A. Yarin, B. Pourdeyhimi, Meltblown fiber mats and their tensile strength, *Polymer* 55 (16) (2014) 4241–4247.
- [33] F. Safaei, S.N. Khorasani, H. Rahnama, R.E. Neisiany, M.S. Koochaki, Single microcapsules containing epoxy healing agent used for development in the fabrication of cost efficient self-healing epoxy coating, *Prog. Org. Coat.* 114 (2018) 40–46.
- [34] F. Ahangaran, M. Hayaty, A.H. Navarchian, Y. Pei, F. Picchioni, Development of self-healing epoxy composites via incorporation of microencapsulated epoxy and mercaptan in poly (methyl methacrylate) shell, *Polym. Test.* 73 (2019) 395–403.
- [35] N. Bhardwaj, S.C. Kundu, Electrospinning: a fascinating fiber fabrication technique, *Biotechnol. Adv.* 28 (3) (2010) 325–347.
- [36] W.I. Lee, A.C. Loos, G.S. Springer, Heat of reaction, degree of cure, and viscosity of Hercules 3501-6 resin, *J. Compos. Mater.* 16 (6) (1982) 510–520.
- [37] M. Naraghi, S. Arshad, I. Chasiotis, Molecular orientation and mechanical property size effects in electrospun polyacrylonitrile nanofibers, *Polymer* 52 (7) (2011) 1612–1618.
- [38] J. Yao, C.W. Bastiaansen, T. Peijs, High strength and high modulus electrospun nanofibers, *Fibers* 2 (2) (2014) 158–186.
- [39] M.W. Lee, S. An, C. Lee, M. Liou, A.L. Yarin, S.S. Yoon, Self-healing transparent core–shell nanofiber coatings for anti-corrosive protection, *J. Mater. Chem. 2* (19) (2014) 7045–7053.
- [40] D.W. Van Krevelen, K. Te Nijenhuis, Properties of Polymers: Their Correlation with Chemical Structure; Their Numerical Estimation and Prediction from Additive Group Contributions, Elsevier, 2009.
- [41] S.-A. Garea, A.-C. Corbu, C. Deleanu, H. Iovu, Determination of the epoxide equivalent weight (EEW) of epoxy resins with different chemical structure and functionality using GPC and 1H-NMR, *Polym. Test.* 25 (1) (2006) 107–113.
- [42] F.G. Garcia, B.G. Soares, Determination of the epoxide equivalent weight of epoxy resins based on diglycidyl ether of bisphenol A (DGEBA) by proton nuclear magnetic resonance, *Polym. Test.* 22 (1) (2003) 51–56.
- [43] W.W. Fleming, Carbon-13 NMR characterization of DGEBA epoxy resins, *J. Appl. Polym. Sci.* 30 (7) (1985) 2853–2862.
- [44] Y. Eom, B.C. Kim, Solubility parameter-based analysis of polyacrylonitrile solutions in N, N-dimethyl formamide and dimethyl sulfoxide, *Polymer* 55 (10) (2014) 2570–2577.
- [45] M.A. Mohammad, A. Alhalaweh, S.P. Velaga, Hansen solubility parameter as a tool to predict cocrystal formation, *Int. J. Pharm.* 407 (1–2) (2011) 63–71.
- [46] R.F. Fedors, A method for estimating both the solubility parameters and molar volumes of liquids, *Polym. Eng. Sci.* 14 (2) (1974) 147–154.